

Momentum Distributions in Halo Nuclei

Jürgen Wurzer* and Hartmut M. Hofmann

Institut für Theoretische Physik III, Staudtstraße 7, Universität Erlangen-Nürnberg, D 91058 Erlangen, Germany

The halo nuclei ${}^6\text{He}$ and ${}^8\text{He}$ are described in a consistent way in a microscopic multiconfiguration model, the refined resonating group method. The ground state properties have been calculated, and momentum distributions of fragments and neutrons have been determined in a simple reaction scenario, taking into account final-state interactions. The correlation of neutrons and fragments are investigated.

PACS-numbers: 21.60.-n, 21.60.Gx, 27.20.+n

I. INTRODUCTION

Nuclear halos – a meanwhile well established phenomena of light neutron rich nuclei – are considered to be roughly understood; and at least the ground state structure of some halo nuclei like ${}^{11}\text{Be}$ and especially ${}^6\text{He}$ are even thought to be almost completely enlightened.

Also the measured momentum distributions of halo nuclei fragments can be described very well within various theoretical models [1-7]. But in all these models some free parameters have been adjusted to reproduce the properties of one nucleus. Contrary to this our aim is a consistent description of a large number of light nuclei, including halo nuclei, within one model whose parameters are fixed once and for all.

First results of this project have been presented in [8] for a consistent description of the nuclei ${}^4\text{He}$ – ${}^8\text{He}$. It turned out that the results for increasing mass number become more and more sensitive to the P -wave part of the employed effective nucleon-nucleon interaction. This part of the potential leads to an overbound ${}^8\text{He}$ indicating a lack of repulsion and hence yielding a too small radius.

In order to cure this problem we removed the odd partial wave part of the effective potential and added a realistic NN interaction with a more repulsive core.

Here we show that with this modified interaction in addition to the lighter isotopes also the heavier isotopes can be described very well in a consistent way, without adjusting any parameter of the interaction to the individual systems.

Besides the ground state properties we compare momentum distributions of fragments and neutrons from ${}^6\text{He}$ and ${}^8\text{He}$ breakup – calculated in sudden approximation and taking into account final-state interactions – with experimental data and calculations in other models. We also discuss the correlation of the halo neutrons.

II. SPATIAL STRUCTURE

All calculations have been performed in a microscopic multiconfiguration cluster model – the refined resonating group method (RRGM). Details of the model are given in [8].

The ${}^6\text{He}$ wave function is a superposition of the (nonorthogonal) clusterings $\alpha(nn)$, $(\alpha n)n$ and tt corresponding to the ${}^4\text{He}+2n$, ${}^5\text{He}+n$ and ${}^3\text{H}+{}^3\text{H}$ thresholds of the ${}^6\text{He}$ system. On the cluster relative coordinates orbital angular momenta $l = 0, 1$ have been allowed for the ${}^6\text{He}$ ground state. Between the nuclei inside the α and triton clusters only $l = 0$ are considered. Four Gaussian functions were employed for the description of each cluster relative wave function and one Gaussian function for the α and the triton cluster each. All Gaussian width parameters have been determined by variation.

TABLE I. Calculated binding energy E_{th} with respect to the ${}^4\text{He}+2n$ threshold, matter r_{m} and charge r_{ch} r.m.s. point nucleon radii for ${}^6\text{He}$ compared with experimental data.

	E_{th} [MeV]	r_{m} [fm]	r_{ch} [fm]
Experiment	0.975 ^[17]	2.33 ± 0.04 ^[18] 2.30 ± 0.07 ^[19]	1.72 ± 0.04 ^[18]
RRGM	0.85	2.47	1.84

In Table I the calculated binding energy with respect to the first threshold and the matter and charge radii are compared with experimental data. The binding energy is about 0.1 MeV to small and hence the radii are a bit too large.

Table II shows the remaining binding energy for the case that one omits each one of the configurations in order to determine the importance of each configuration. Without the $(\alpha n)n$ clustering with P -waves on both cluster relative coordinates (the ${}^5\text{He}$ g.s. + n configuration) the binding is lost. Omitting the triton-triton clustering decreases the binding considerable, which is surprising because of the high threshold but in agreement with the calculations of Csótó [9]. Omitting any one of the other configurations effects the binding energy hardly at all.

*e-mail: jwurzer@theorie3.physik.uni-erlangen.de

TABLE II. Remaining binding energy for ${}^6\text{He}$ omitting each one of the configurations.

omitted configuration		E_{th} [MeV]
none		0.85
$(\alpha n)n$	$l_{1,2}=0$	0.81
$(\alpha n)n$	$l_{1,2}=1$	unbound
tt	$l=0$	0.22
$\alpha(nn)$	$l_{1,2}=0$	0.81
$\alpha(nn)$	$l_{1,2}=1$	0.67

The P -state probability is 14.1 % and thus in agreement with a hyperspherical harmonics calculation [12].

The ${}^8\text{He}$ wave function is a superposition of the (nonorthogonal) clusterings $(\alpha(nn))(nn)$ with $l = 0$ on all coordinates, $((\alpha n)n)n$ with $l = 1$ on all coordinates, $((\alpha n)n)(nn)$ with $l = 1$ to the n clusters and $l = 0$ to the nn cluster, $((\alpha nn))n$ with $l = 1$ to the n clusters and $l = 0$ to the nn cluster, and $((tt)n)n$ with $l = 0$ on all coordinates and in addition also $l = 0$ between the t clusters and $l = 1$ to the n clusters.

The calculated binding energy with respect to the ${}^4\text{He}+4n$ threshold and the matter and charge radii are in good agreement with experimental data (cf. Table III).

TABLE III. Calculated binding energy E_{th} with respect to the ${}^4\text{He}+4n$ threshold, matter r_{m} and charge r_{ch} r.m.s. point nucleon radii for ${}^8\text{He}$ compared with experimental data.

	E_{th} [MeV]	r_{m} [fm]	r_{ch} [fm]
Experiment	3.112 ^[17]	2.49 ± 0.04 ^[18]	1.76 ± 0.03 ^[18]
		2.45 ± 0.07 ^[19]	
RRGM	2.99	2.41	1.71

The most important configuration for the binding energy is $((\alpha n)n)n$ (cf. Table IV). The contribution of the $((tt)n)n$ channel is substantial. The P -state probability is 49.8 %. We omitted the D -states totally since it turned out that they contribute only a few keV to the binding energy.

Both wave functions are determined with the same NN interaction by a variational principle. For the even partial waves the effective potential of Stöwe and Zahn [10],

TABLE IV. Remaining binding energy with respect to the ${}^4\text{He}+4n$ threshold for ${}^8\text{He}$ omitting each one of the configurations.

omitted configuration	E_{th} [MeV]
none	2.99
$(\alpha(nn))(nn)$	2.97
$((\alpha n)n)n$	unbound
$((\alpha n)n)(nn)$	2.96
$((\alpha nn))n$	2.96
$((tt)n)n$	2.36

for the odd partial waves the realistic interaction of Eike-meier and Hackenbroich [11] has been employed. Both contain Coulomb, nuclear central, spin-orbit, and tensor components. The strength of the spin-orbit force was increased by a factor of 2.5.

III. MOMENTUM DISTRIBUTIONS AND SPATIAL CORRELATIONS

In the simple picture of the serber model (sudden approximation) [13] in which any influence of the reaction mechanism of the fragmentation and the final-state interaction is neglected, the measured momentum distribution is given by the Fourier transformation of the relative wave function between the fragments integrated over the not observed momentum coordinates:

$$\frac{dN}{dP_x} \propto \int dP_y dP_z \rho_{\phi_1\phi_2}(\mathbf{P}), \quad (1)$$

with

$$\rho_{\phi_1\phi_2}(\mathbf{P}) = \left| \frac{1}{(2\pi\hbar)^{3/2}} \int d\mathbf{R} \Psi_{\text{rel}}(\mathbf{R}) \exp\left(\frac{i}{\hbar}\mathbf{R}\mathbf{P}\right) \right|^2. \quad (2)$$

The totally antisymmetrized relative wave function between the fragments $|\phi_1\rangle$ and $|\phi_2\rangle$ is calculated as an overlap with the total wave function $|\phi_3\rangle$ where the integration is performed over all coordinates except the relative coordinate \mathbf{r} between the two fragments:

$$\Psi_{\text{rel}}(\mathbf{R}) = \langle \phi_1\phi_2 | \delta(\mathbf{r} - \mathbf{R}) \mathcal{A} | \phi_3 \rangle. \quad (3)$$

In this sense the relative wave function is projected out of the multiconfiguration total wave function. This is necessary since the different configurations are not orthogonal. \mathcal{A} denotes the antisymmetrization operator.

The relative wave function can be projected onto a certain orbital angular momentum L :

$$\Psi_{\text{rel}}^L(\mathbf{R}) = Y_{LL}(\hat{\mathbf{R}}) \int d\hat{\mathbf{R}}' Y_{LL}^*(\hat{\mathbf{R}}') \Psi_{\text{rel}}(\mathbf{R}'). \quad (4)$$

In the common reaction scenario one of the halo neutrons is removed by the target and scattered to large angles and therefore not detected. This picture is based on the average neutron multiplicity measured to be close to one [16]. The remaining second neutron and the core may form a short living resonant state. The measured momentum distribution of the products of the decay of this resonance are thus no more only determined by their original, internal motion in the halo nucleus. Rather the final-state interaction has, at least in some cases, an important influence. The modification of the internal momentum distribution by the final-state interaction can be described [3,7,16] by using a Breit-Wigner formula,

$$I_{\text{BW}} = \frac{1}{2\pi} \frac{\Gamma}{(E - E_{\text{res}})^2 + \Gamma^2/4}, \quad (5)$$

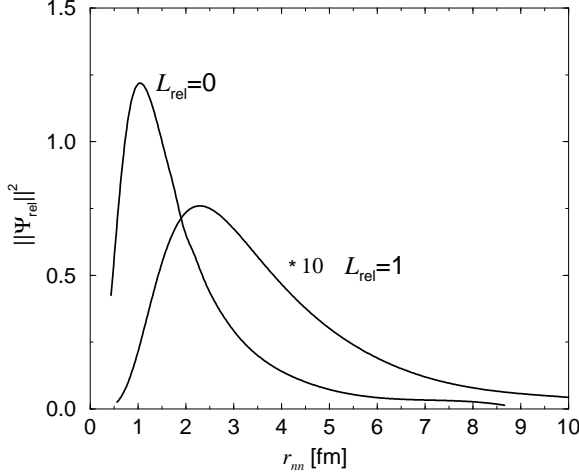


FIG. 1. Square of the norm of the projected relative wave function $\|\Psi_{\text{rel}}^L\|^2$ as a function of the r.m.s. radius of $|nn\rangle$.

with resonance energy E_{res} and width Γ .

For the calculation of the momentum distribution of the ${}^4\text{He}$ fragments from ${}^6\text{He}$ breakup one has $|\phi_1\rangle = |{}^4\text{He}\rangle$, $|\phi_2\rangle = |nn\rangle$ and $|\phi_3\rangle = |{}^6\text{He}\rangle$. The $|{}^4\text{He}\rangle$ function was determined by variation and has, in good agreement with experimental data, a point nucleon root mean square radius of 1.42 fm. The α cluster radii inside $|{}^6\text{He}\rangle$ are very similar to this value but the momentum distribution is not very sensitive to it.

To determine the function $|nn\rangle$ and thus the correlation of the two halo neutrons in ${}^6\text{He}$ we took the norm of the projected relative wave function $\|\Psi_{\text{rel}}\|$ as a measure of the content of a certain $|nn\rangle$ configuration in $|{}^6\text{He}\rangle$ for a fixed $|{}^4\text{He}\rangle$ fragment. Figure 1 shows $\|\Psi_{\text{rel}}^L\|^2$ as a function of the root mean square radius of $|nn\rangle$ which is a good parametrization of the simple Gaussian function which has been used for the \mathbf{r} -space representation of $|nn\rangle$. The two pronounced peaks in Fig. 1, at 1.0 fm for $L_{\text{rel}} = 0$ and at 2.3 fm for $L_{\text{rel}} = 1$, correspond to a spatially strongly correlated dineutron configuration and a spatially strongly anticorrelated cigar-like neutron pair. This observation is in agreement with the results of a hyperspherical harmonics calculation (HH) [12].

The $|nn\rangle$ configurations with maximal $\|\Psi_{\text{rel}}^L\|$ have been chosen for the calculation of $\Psi_{\text{rel}}(\mathbf{R})$. The resulting momentum distribution for ${}^4\text{He}$ fragments in sudden approximation is compared in Fig. 2 with the measured transverse momentum distribution [14] and a calculation in a HH model [12] where also the approximation of the serber model was used. Both theoretical curves are in good agreement with the experiment. This indicates that, besides the fulfilled preconditions for the serber model, high energy, light target and a loosely bound projectile, the ${}^4\text{He}n$ final-state interaction hardly effects the ${}^4\text{He}$ momentum distribution. Also the ${}^4\text{He}$ target interaction seems to play no important role for the detected ${}^4\text{He}$

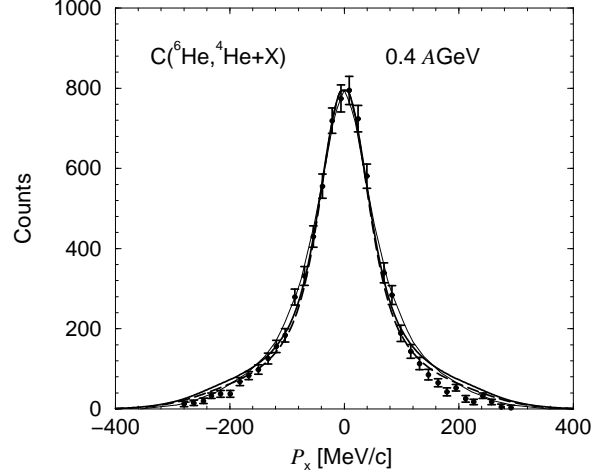


FIG. 2. ${}^4\text{He}$ transverse momentum distribution from a ${}^6\text{He}$ breakup calculated in the RRGM with final state interactions (thick solid line) and in sudden approximation (dashed line) in comparison with experimental data [14] and the HH model [12] in sudden approximation (thin solid line).

fragments.

Taking final-state interactions into account, the ${}^4\text{He}$ transverse momentum distribution is given by

$$\frac{dN_{{}^4\text{He}}^{\text{FSI}}}{dP_x} \propto \int dP_y dP_z \int d\mathbf{P}' d\mathbf{P}'' \rho_{{}^4\text{He}(nn)}(\mathbf{P}) I_{\text{BW}}(\mathbf{P}') \delta(\mathbf{P}' + \frac{4}{5}\mathbf{P}'' + \mathbf{P}), \quad (6)$$

where \mathbf{P}'' is the momentum of the removed neutron and \mathbf{P} the ${}^4\text{He}$ momentum, both in the ${}^6\text{He}$ c.m. system (cf. Fig. 3). \mathbf{P}' is the relative momentum of the detected neutron and the ${}^4\text{He}$ fragment in the ${}^5\text{He}$ c.m. system, connected with E from Eq. (5) by

$$E = \frac{P'^2}{2\frac{5}{4}m}, \quad (7)$$

with the nuclear mass m . We used $E_{\text{res}} = 0.89$ MeV and $\Gamma = 0.6$ MeV in Eq. (5) for the ${}^5\text{He}$ ground state resonance [17]. Indeed Fig. 2 shows that the final-state

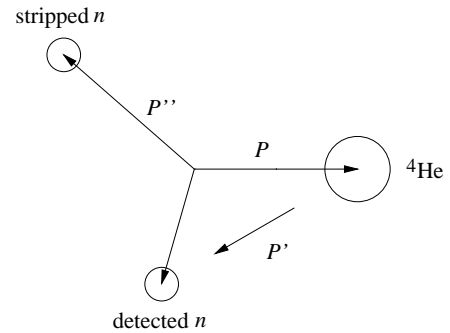


FIG. 3. Definition of the momenta appearing in Eq. (6).

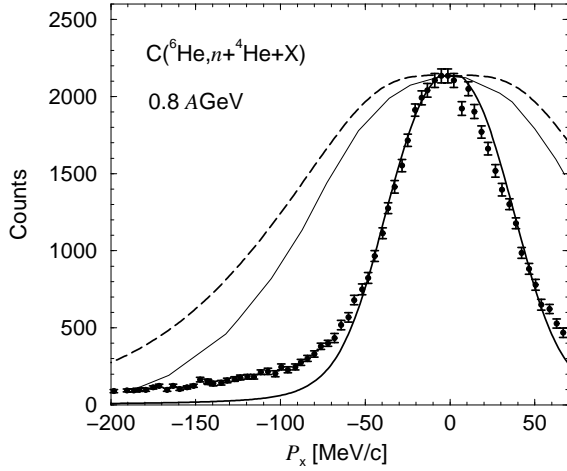


FIG. 4. Neutron transverse momentum distribution from a ${}^6\text{He}$ breakup calculated in the RRGm with final state interactions (thick solid line) and in sudden approximation (dashed line) in comparison with experimental data [15] and the HH model [5] in sudden approximation (thin solid line).

interaction does almost not effect the momentum distribution of the ${}^4\text{He}$ fragments.

In order to calculate the neutron momentum distribution one has to employ $|\phi_1\rangle = |{}^5\text{He}\rangle$ and $|\phi_2\rangle = |n\rangle$. The wave function for the unbound system $|{}^5\text{He}\rangle$ was constructed in the same way as for the dineutron $|nn\rangle$. The maximum of $\|\Psi_{\text{rel}}\|$ was determined with respect to the relative wave function between the α cluster and the neutron in $|{}^5\text{He}\rangle$ for a fixed α . In this sense the mean value of the α core halo neutron radius inside ${}^6\text{He}$ was determined to 2.0 fm. The corresponding momentum distribution (cf. Fig. 4) in sudden approximation is much broader than the measured transverse neutron momentum distribution [15] but in agreement with a three-body calculation in the serber model [5].

Some different processes might be responsible for this discrepancy. The ${}^4\text{He}n$ final-state interaction is considered to be the most dominant one [5]. But moreover, in contrast to the ${}^4\text{He}$ fragments the detected neutrons might have different origins: they could be emitted from the neutron halo by a direct breakup or with a target interaction, they could be emitted from the ${}^4\text{He}$ core or even from the target itself [5].

Taking final-state interactions into account, the neutron transverse momentum distribution is given by

$$\frac{dN_n^{\text{FSI}}}{dP_x} \propto \int dP_y dP_z \int d\mathbf{P}' d\mathbf{P}'' \rho_{{}^5\text{He}n}(\mathbf{P}'') I_{\text{BW}}(\mathbf{P}') \delta(\mathbf{P}' - \mathbf{P} - \frac{1}{5}\mathbf{P}''), \quad (8)$$

where \mathbf{P} is the momentum of the detected neutron. The meaning of \mathbf{P}' and \mathbf{P}'' is the same as in Eq. 6 (cf. Fig. 3). Contrary to the ${}^4\text{He}$ fragment, the neutron momentum

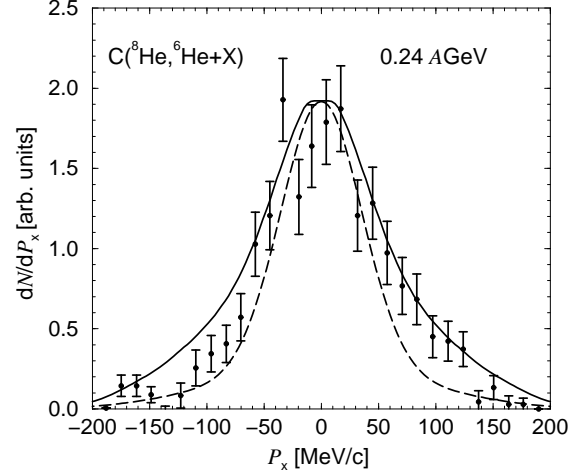


FIG. 5. ${}^6\text{He}$ transverse momentum distribution from ${}^8\text{He}$ breakup calculated in the RRGm with final-state interactions (solid line) and in sudden approximation (dashed line) in comparison with experimental data [16].

distribution is considerably influenced by the final-state interaction (cf. Fig. 4). The distribution (8) is in good agreement with the measured distribution. The remaining discrepancy beyond 60 $\frac{\text{MeV}}{c}$ might be due to neglecting the neutron target interaction [5].

The momentum distribution for ${}^6\text{He}$ fragments from ${}^8\text{He}$ breakup was calculated in a way analogical to the determination of the ${}^4\text{He}$ distribution from ${}^6\text{He}$ breakup: The determination of maxima of $\|\Psi_{\text{rel}}^L\|$ showed that the second halo neutron pair has a strong correlated component with a root mean square radius of 1.2 fm for spin $s = 0$ and a less correlated component with a radius of 1.8 fm for spin $s = 1$. The momentum distribution for ${}^6\text{He}$ fragments calculated in the RRGm model in sudden approximation seems to be a bit too narrow but is still compatible with the measured transverse momentum distribution [16] (cf. Fig. 5).

Taking final-state interactions into account, the ${}^6\text{He}$ transverse momentum distribution is given by

$$\frac{dN_{{}^6\text{He}}^{\text{FSI}}}{dP_x} \propto \int dP_y dP_z \int d\mathbf{P}' d\mathbf{P}'' \rho_{{}^6\text{He}({}^6\text{He})}(\mathbf{P}) I_{\text{BW}}(\mathbf{P}') \delta(\mathbf{P}' + \frac{6}{7}\mathbf{P}'' + \mathbf{P}), \quad (9)$$

where the momenta \mathbf{P} , \mathbf{P}' and \mathbf{P}'' are defined analogically to Eq. (6).

For the parameters E_{res} and Γ in Eq. (5) we employed not only the experimental values for the ${}^7\text{He}$ ground state resonance (0.44 MeV and 0.16 MeV) [17] but also the results of an S-matrix analysis of the phase shifts calculated in the RRGm (0.442 MeV and 0.114 MeV) in [8]. The resulting momentum distributions differ only within the line width in Fig. 5 and 6. It is shown in Fig. 5 that the final-state interaction increases the width of the ${}^6\text{He}$

IV. SUMMARY

It was shown that the ground state properties of halo nuclei and the momentum distributions of fragments and neutrons from breakup reactions can be well reproduced in a consistent way in the microscopic description of the refined resonating group method. The momentum distributions of ^4He and ^6He fragments from ^6He and ^8He breakup, respectively, are in good agreement with the measured distributions and almost not influenced by final-state interactions. On the contrary, the neutron momentum distributions can only be explained by taking final-state interactions into account.

ACKNOWLEDGMENTS

This work was supported by DFG and BMBF.

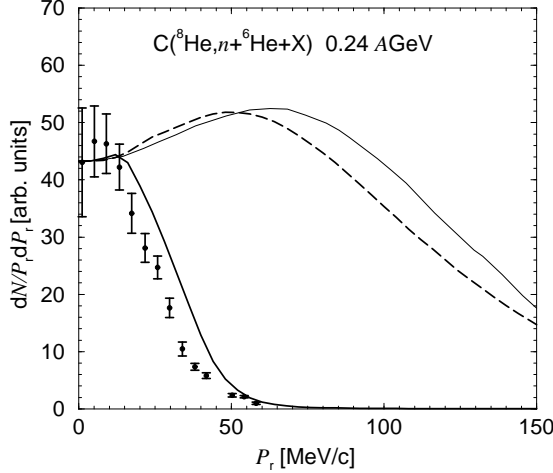


FIG. 6. Neutron radial momentum distribution from ^8He breakup calculated in the RRGm with final-state interactions (thick solid line) and in sudden approximation (dashed line) in comparison with experimental data [16] and COSMA calculation [16] in sudden approximation (thin solid line).

momentum distribution in such a way as to yield good agreement with the measured one.

The neutron momentum distribution was calculated by setting $|\phi_1\rangle = |^7\text{He}\rangle$ and $|\phi_2\rangle = |n\rangle$. The maximum of $\|\Psi_{\text{rel}}\|$ was determined with respect to the relative wave function between the ^6He function and the neutron in $|^7\text{He}\rangle$ for a fixed ^6He . The mean value of the $^6\text{He}n$ radius was determined to 2.3 fm. Contrary to Eq. (1) the momentum distribution for neutrons from ^8He breakup has been calculated by integration only over one momentum coordinate in order to compare with experimental data [16]. The RRGm and the COSMA calculations [16] in sudden approximation are in good agreement (cf. Fig. 6) with each other but much broader than the measured radial momentum distribution. This discrepancy is presumable due to the same reasons as for the ^6He breakup.

Taking final-state interactions into account, the neutron radial momentum distribution is given by

$$\frac{dN_n^{\text{FSI}}}{P_r dP_r} \propto \int dP_z \int dP' dP'' \rho_{^7\text{He}n}(P'') I_{\text{BW}}(P') \delta(P' - P - \frac{1}{7}P''). \quad (10)$$

The momenta P , P' and P'' are defined analogically to Eq. (8). The extracted width of $66 \frac{\text{MeV}}{c}$ is a little larger than the measured one of $54 \frac{\text{MeV}}{c}$ (cf. Fig. 6).

The origin of this small deviation from the experimental data is not obvious. The width of the distribution given by Eq. (10), however, depends very strongly on the position of the ^7He resonance but not on the resonance width. For example lowering the parameter E_{res} in Eq. (5) by about 100 keV yields perfect agreement with the data (see also [16]).

- [1] P.G. Hansen, Phys. Rev. Lett. **77**, 1016 (1996).
- [2] H. Esbensen, Phys. Rev. C **53**, 2007 (1996).
- [3] A.A. Korshennikov, M.V. Zhukov, M.H. Smedberg and T. Kobayashi, Europhys. Lett. **29**, 359 (1995).
- [4] Y. Suzuki, K. Arai, Y. Ohbayasi and K. Varga, Nucl. Phys. A **588**, 15c (1995).
- [5] A.A. Korshennikov and T. Kobayashi, Nucl. Phys. A **567**, 97 (1994).
- [6] K. Varga, Y. Suzuki and Y. Ohbayasi, Phys. Rev. C **50**, 189 (1994).
- [7] M.V. Zhukov, A.A. Korshennikov and M.H. Smedberg, Phys. Rev. C **50**, R1 (1994).
- [8] J. Wurzer and H.M. Hofmann, Phys. Rev. C **55**, 688 (1997).
- [9] A. Cs6t6, Phys. Rev. C **48**, 165 (1993).
- [10] T. Mertelmeier and H.M. Hofmann, Nucl. Phys. A **459**, 387 (1986).
- [11] H. Eikemeier and H.H. Hackenbroich, Nucl. Phys. A **169**, 407 (1971).
- [12] M.V. Zhukov, L.V. Chulkov, B.V. Danilin and A.A. Korshennikov, Nucl. Phys. A **533**, 428 (1991).
- [13] R. Serber, Phys. Rev. **72**, 1008 (1947); Annu. Rev. Nucl. Part. Sci. **44**, 1 (1994).
- [14] T. Kobayashi, Nucl. Phys. A **538**, 343c (1992).
- [15] T. Kobayashi, Nucl. Phys. A **553**, 465c (1993).
- [16] T. Nilsson *et al.*, Nucl. Phys. A **598**, 418 (1996).
- [17] F. Ajzenberg-Selove, Nucl. Phys. A **490**, 1 (1988).
- [18] I. Tanihata *et al.*, Phys. Lett. B **289**, 261 (1992).
- [19] G.D. Alkhazov *et al.*, Phys. Rev. Lett. **78**, 2313 (1997).